Supporting Information

for

Experimental and theoretical characterization of Rh single-atoms supported on γ-Al_2O_3 with varying hydroxyl content during NO reduction by CO

Alexander J. Hoffman[1†], Chithra Asokan[2†], Nicholas Gadinas[2], Emily Schroeder,[2] Gregory Zakem,[2] Steven V. Nystrom[1], Andrew "Bean" Getsoian[3], Phillip Christopher[2]*, David Hibbitts[1]*

[1]Department of Chemical Engineering, University of Florida, Gainesville, FL 32611, USA

[2]Department of Chemical Engineering, University of California Santa Barbara, Santa Barbara, CA 93106, USA

[3]Research and Advanced Engineering, Ford Motor Company, Dearborn, MI 48124, USA

[†]A.J.H. and C.A. contributed equally to this work.

*Corresponding authors: pchristopher@ucsb.edu, hibbitts@che.ufl.edu

Table of Contents

List of Figures and Tables

S1. Additional computational details

Enthalpies (*H*) and Gibb's free energies (*G*) can be calculated from density functional theory (DFT)-derived energies using statistical mechanics. Specifically, each is a sum of the electronic energy (E_0), the zero-point vibrational energy (ZPVE), and the respective vibrational, translational, and rotational components of the species:

$$H = E_o + ZPVE + H_{vib} + H_{rot} + H_{trans} \quad \text{(S1)}$$

$$G = E_0 + ZPVE + G_{vib} + G_{rot} + G_{trans} \quad \text{(S2)}$$

at 473 K. Adsorbed species are not considered to have translational or rotational contributions; all such motions are modeled as frustrated vibrations on the surface. Metal atoms of the Rh(111) surfaces and on the Rh_{201} nanoparticles are frozen in place during frequency calculations. All atoms of the support were frozen during frequency calculations on γ-Al_2O_3, while atoms attached to the support (the Rh single-atom and species bound to it; H and OH bound to the γ-Al_2O_3 support) were unfrozen. Vibrational, rotational, and translational enthalpies and free energies are estimated from other statistical mechanics formalisms:

$$ZPVE = \sum_i \left(\frac{1}{2} h\nu_i\right) \quad \text{(S3)}$$

$$H_{vib} = \sum_i \left(\frac{h\nu_i \exp\left(-\frac{h\nu_i}{kT}\right)}{1 - \exp\left(-\frac{h\nu_i}{kT}\right)} \right) \quad \text{(S4)}$$

$$G_{vib} = \sum_i \left(-kT \ln \left(\frac{1}{1 - \exp\left(-\frac{h\nu_i}{kT}\right)} \right) \right) \quad \text{(S5)}$$

$$H_{trans} = \frac{5}{2} kT \quad \text{(S6)}$$

$$H_{rot,linear} = kT \quad \text{(S7)}$$

$$H_{rot,nonlinear} = \frac{3}{2} kT \quad \text{(S8)}$$

$$G_{trans} = -kT \ln \left(\left(\frac{2\pi mkT}{h^2} \right)^{\frac{3}{2}} V \right) \quad \text{(S9)}$$

$$G_{rot} = -kT \ln \left(\frac{\pi^{\frac{1}{2}}}{\sigma} \left(\frac{T^3}{\theta_x \theta_y \theta_z} \right)^{\frac{1}{2}} \right) \quad \text{(S10)}$$

$$\theta_i = \frac{h^2}{8\pi^2 I_i k} \quad \text{(S11)}$$

where I_i is the moment of intertia about the *i* axis (either x, y, or z) and σ is the symmetry number of the species.[1]

S2. Models of γ-Al_2O_3 employed

All surface models of γ-Al_2O_3 used in this work were developed from the structure first published by Digne et al.[2–5] The unit cell of this γ-Al_2O_3 model contained 8 Al_2O_3 units. Surface formation energies were calculated by adding 10 Å of vacuum above various terminations of the preferred surfaces of γ-Al_2O_3. All surface models contained four times the number of Al_2O_3 units as in the bulk (32 Al_2O_3 units) and were fully dehydrated. Therefore, the surface formation energy was calculated as

$$\Delta E_{surf} = \frac{1}{A}(4 * E_{bulk} - E_{surface}) \quad \text{(S12)}$$

where A is the area of the exposed surface, E_{bulk} is the energy of the bulk γ-Al_2O_3, and E_{surface} is the energy of the surface. The surface energies for the models used in this work are shown in Table S1. The $(001)_b$ surface has the lowest formation energy, likely because the exposed Al on this facet are most highly coordinated among all those tested in this work. Moreover, the Lewis acidity of the Al of the $(100)_b$ and $(010)_b$ facets of this γ-Al_2O_3 model is well-established, and these two facets bind OH groups derived from H_2O during the dehydration of boehmite up to 800 K. [2] As such, the bare $(100)_b$ and $(010)_b$ facets are likely to be more stable when covered with OH groups and XRD[1] and computational[2] data indicate that these facets are more common than $(001)_b$.

Table S1. Surface formation energies for the most stable termination of the facets of γ-Al_2O_3 tested in this work from the model developed by Digne et al.[2,3]

γ-Al_2O_3 facet	Corresponding boehmite facet	ΔE_{surf} (kJ mol^{-1} Å^2)
$(110)_{cds}$	$(100)_b$	13.2
$(110)_{cds}$	$(010)_b$	12.2
$(100)_{cds}$	$(001)_b$	7.3

The structures of these γ-Al_2O_3 models absent water are shown in Figure 1 of the main text and compared with models from a cubic defect spinel (cds) model based on XRD studies of γ-Al_2O_3.[6] The images of the cds model in the main text are not optimized, simply the structures of the initial cleaved surfaces. Upon optimization, these surfaces restructure significantly (Fig. S1), indicating the instability of these models and their inappropriateness for density functional theory (DFT) studies of catalysts supported on γ-Al_2O_3.

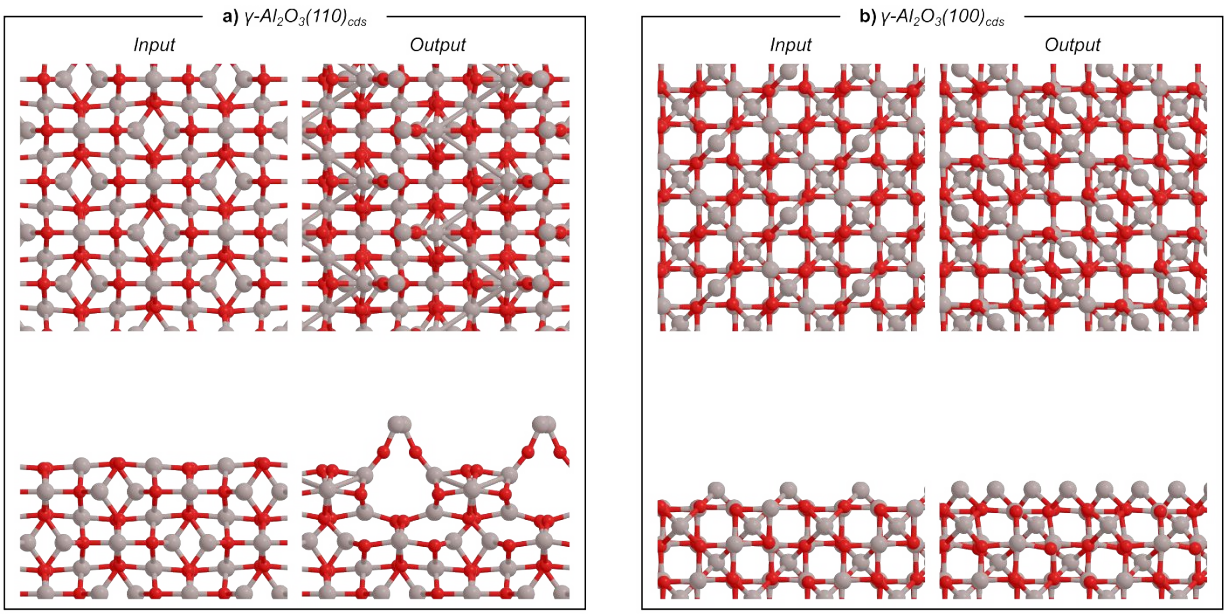

Figure S1. Initial and optimized surfaces for the most stable terminations of (**a**) γ-$Al_2O_3(110)_{cds}$ and (**b**) γ-$Al_2O_3(100)_{cds}$ derived from the cubic defect spinel model based on XRD studies.[6]

Additional views of the γ-Al_2O_3 models employed in this work are shown in Figure S2. A 10 Å vacuum layer was added above each surface. The bottom half of each slab was frozen during optimization calculations (corresponding to 160, 80, and 80 frozen atoms for the $(100)_b$, $(010)_b$, and $(001)_b$ slabs, respectively). The slabs for the $(100)_b$, $(010)_b$, and $(001)_b$ surfaces are 11.85, 7.07, and 16.36 Å thick, respectively.

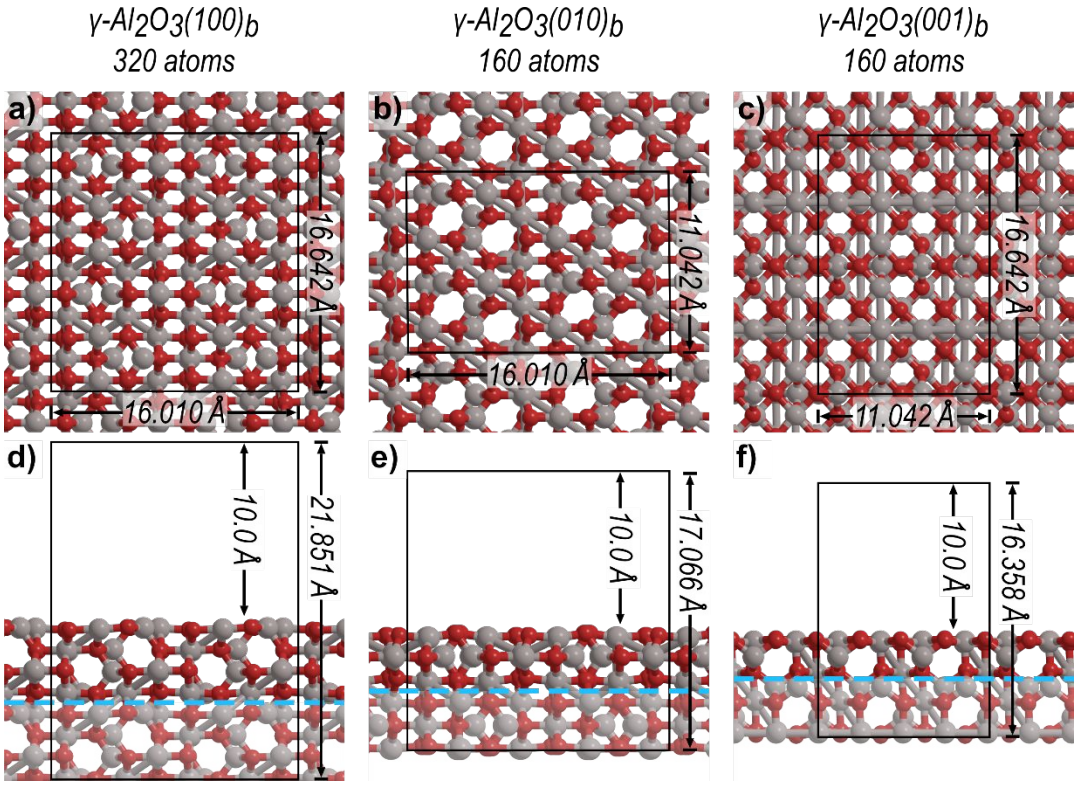

Figure S2. Detailed views of the γ-Al_2O_3 models used in this work for (**a, d**) the $(100)_b$, (**b, e**) the $(010)_b$, and (**c, f**) the (001)b surfaces shown (**a–c**) perpendicular to and (**d–f**) parallel to the surface. The total number of atoms in each γ-Al_2O_3 is shown above the respective structure. The horizonal dashed light blue lines in **d–f** indicate the point below which atoms were frozen during optimization calculations.

S3. IR spectra for identification of NCO*

In situ IR spectra of atomically dispersed Rh/γ-Al_2O_3 contain features near 2250 and 2230 cm^{-1} that have been assigned to adsorbed isocyanate species (NCO*).[7,8] We confirm that Rh exists predominantly as $Rh(CO)_2$ by collecting a series of IR spectra to demonstrate that Rh is saturated with CO during reaction conditions (Fig. S2a), that the features near 2250 and 2230 cm^{-1} correspond to NCO* rather than N_2O* (Fig. S2b), and that NCO* is spilling over onto the support rather than sitting on Rh sites (Fig. S2c).

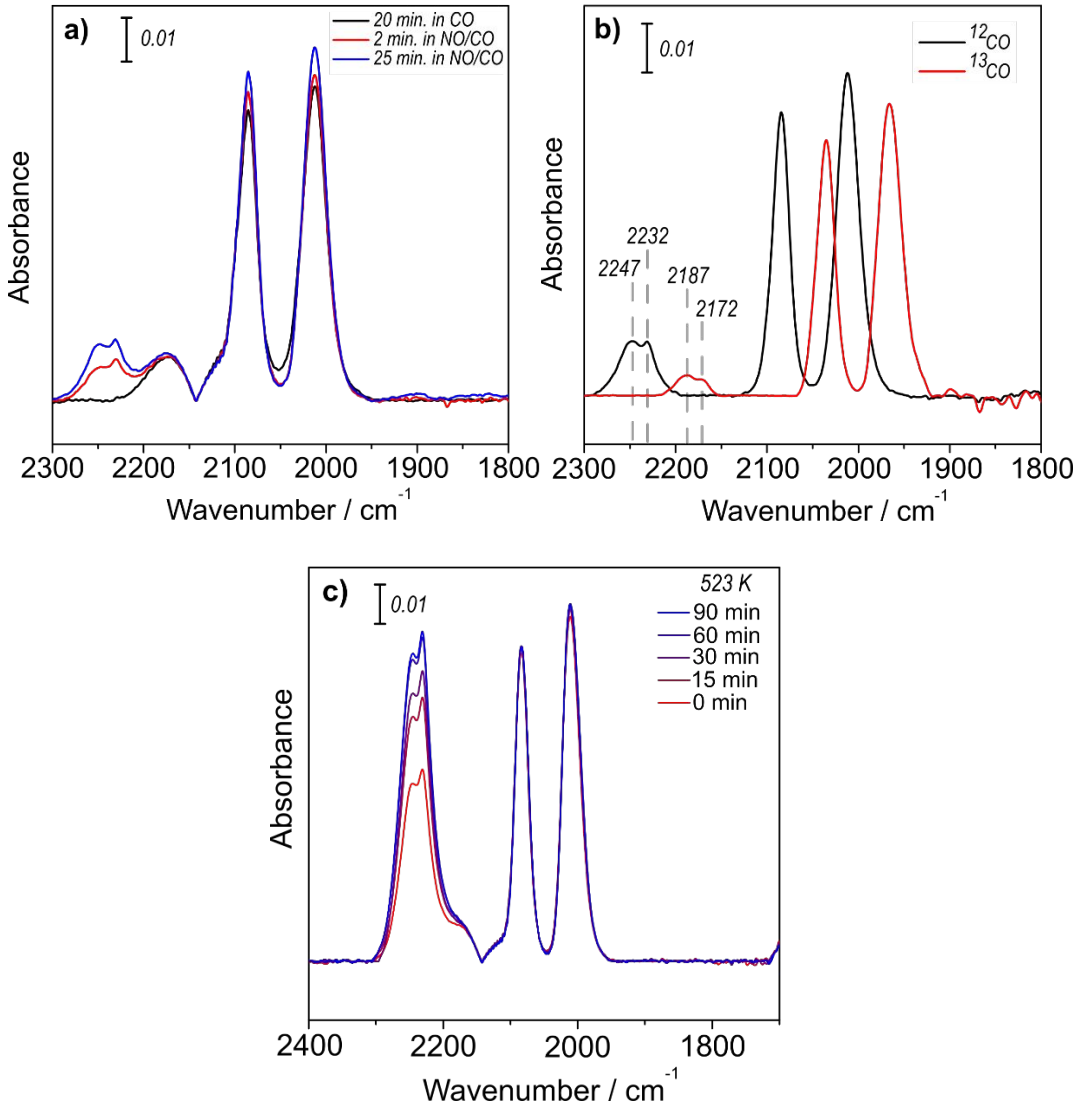

Figure S3. IR spectra of 0.05 wt.% Rh/γ-Al_2O_3 (**a**) after saturation with 0.5 kPa CO for 20 min (black), during exposure to 0.5 kPa CO and 0.1 kPa NO after 2 min (red) and 25 min (blue) at 463 K; (**b**) after 25 minutes in 0.5 kPa ^{12}CO and 0.1 kPa NO at 463 K (purged with Ar) (black) and after saturation with 10 kPa ^{13}CO and a pulse of 1 kPa NO at 463 K (purged with Ar) (red); and (**c**) during exposure to 0.5 kPa CO and 0.1 kPa NO at 523 K after exposure to the same mixture at 473 K. All gas mixtures were balanced with Ar to 1 bar.

S4. IR spectra for cooled Rh/γ-Al_2O_3 sample after temperature-programmed desorption

We investigated the resulting Rh structure produced following the thermal desorption of CO from atomically dispersed $Rh(CO)_2$ complexes by cooling down to cryogenic temperature and re-exposing the catalyst to CO after conducting the temperature-programmed desorption (TPD). Cryogenic temperature was used to ensure that CO-induced fragmentation or restructuring of Rh complexes was minimized. During the TPD, the catalyst was heated at 0.33 K s^{-1} (20 K min^{-1}) from 298 K to 623 K, at which a significant portion of $Rh(CO)_2$ disappeared and the new shoulder at 1985/1975 cm^{-1} assigned to Rh(CO) appeared. The catalyst was then cooled to 143 K and CO was introduced to the cell for 20 minutes before purging with Ar.

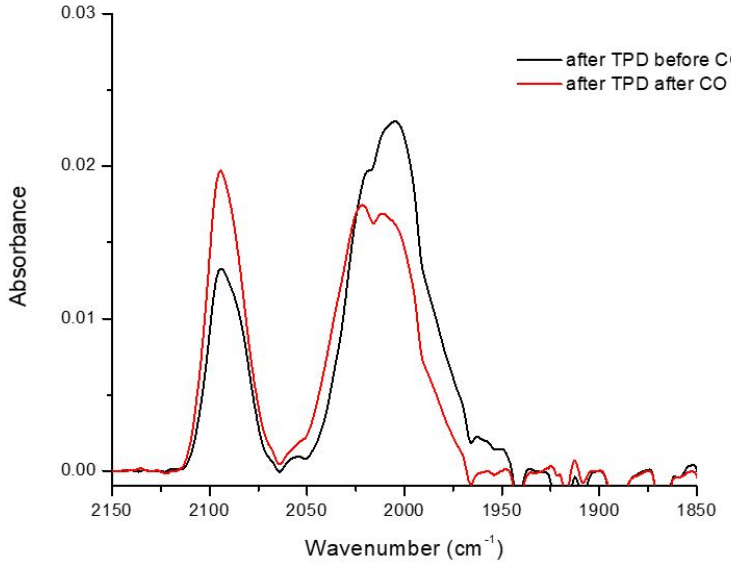

Figure S4. CO-DRIFTS spectra of 0.2 wt% Rh/Al_2O_3 collected after TPD with heating from 298 to 623 K at 0.33 K s^{-1} and cooling to 183 K in Ar (black), and again after flowing 10% CO in Ar for 1200 s at 143 K and purging to collect a final spectrum at 183 K (red).

S5. DFT calculations with different OH coverages on γ-Al_2O_3

The coverages of adsorbed water can be estimated based on equilibrium constants ($K_{W,x}$) from H_2O adsorption free energies ($\Delta G_{W,x}$) at 1 bar (standard pressure) and 473 K:

$$K_{W,x} = e^{-\frac{\Delta G_{W,x}}{kT}} = e^{-\frac{\Delta H_{W,x} - T\Delta S_{W,x}}{kT}} \quad \text{(S12)}$$

where x is the number of H_2O that have adsorbed, $\Delta H_{W,x}$ is the enthalpy of adsorption, and $\Delta S_{W,x}$ is the entropy of adsorption for the x^{th} H_2O. These can then be applied to the Langmuirian adsorption isotherm to predict the coverage of OH groups at a range of temperatures (T) and water pressures (P_W):

$$\theta_W = \left(\frac{1}{A}\right)\frac{\sum_i i K_{W,i} P_W^i}{\sum_j K_{W,j} P_W^i} \quad \text{(S13)}$$

where A is the surface area of the unit cell of the γ-Al_2O_3 surface to give coverage in units of OH nm^{-2} and i and j are the number of adsorbed H_2O.

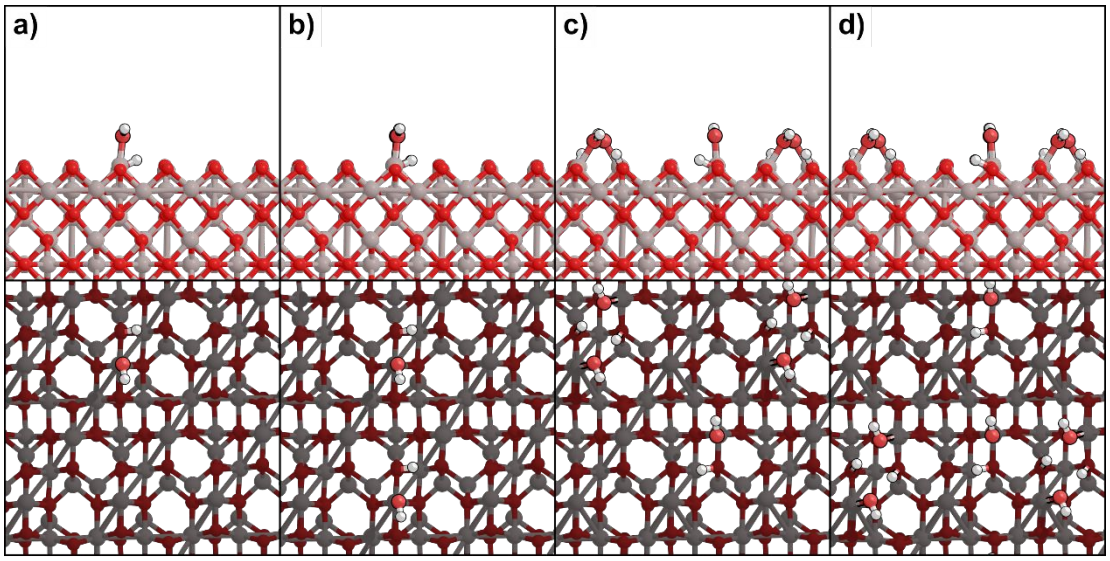

	1.13 OH nm^{-2} 0.00 H_2O nm^{-2}	2.26 OH nm^{-2} 0.00 H_2O nm^{-2}	3.39 OH nm^{-2} 0.00 H_2O nm^{-2}	4.53 OH nm^{-2} 0.00 H_2O nm^{-2}
ΔH_W	−141	−145	−127	−142
ΔG_W	−66	−71	−51	−69
ΔS_W	−157	−156	−160	−156

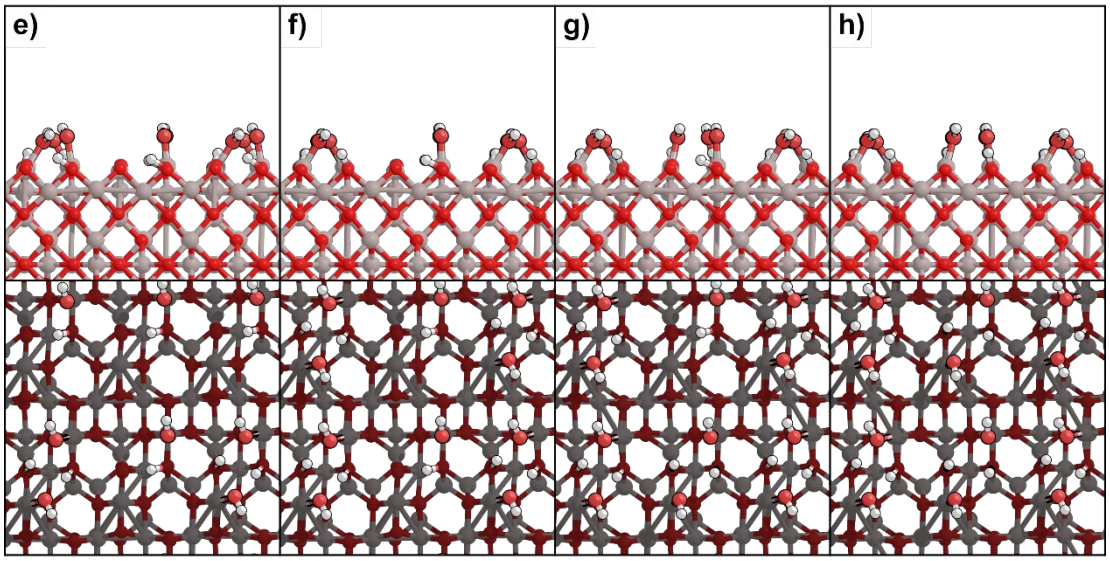

	5.66 OH nm^{-2} 0.00 H_2O nm^{-2}	6.79 OH nm^{-2} 0.00 H_2O nm^{-2}	7.92 OH nm^{-2} 0.00 H_2O nm^{-2}	9.05 OH nm^{-2} 0.00 H_2O nm^{-2}
ΔH_W	−128	−137	−120	−123
ΔG_W	−57	−59	−50	−51
ΔS_W	−149	−164	−148	−151

Figure S5. γ-Al_2O_3 with dissociatively adsorbed H_2O at (**a**) 1.13 OH nm^{-2}, (**b**) 2.26 OH nm^{-2}, (**c**) 3.39 OH nm^{-2}, (**d**) 4.53 OH nm^{-2}, (**e**) 5.66 OH nm^{-2}, (**f**) 6.79 OH nm^{-2}, (**g**) 7.92 OH nm^{-2}, and (**h**) 9.05 OH nm^{-2} (from 1-8 dissociatively adsorbed H_2O molecules), shown parallel (top) and perpendicular (bottom) to the surface. Adsorption enthalpies (ΔH_W) and free energies (ΔG_W) in kJ mol^{-1} and entropies (ΔS_W) in J mol^{-1} K^{-1} are shown beneath each structure.

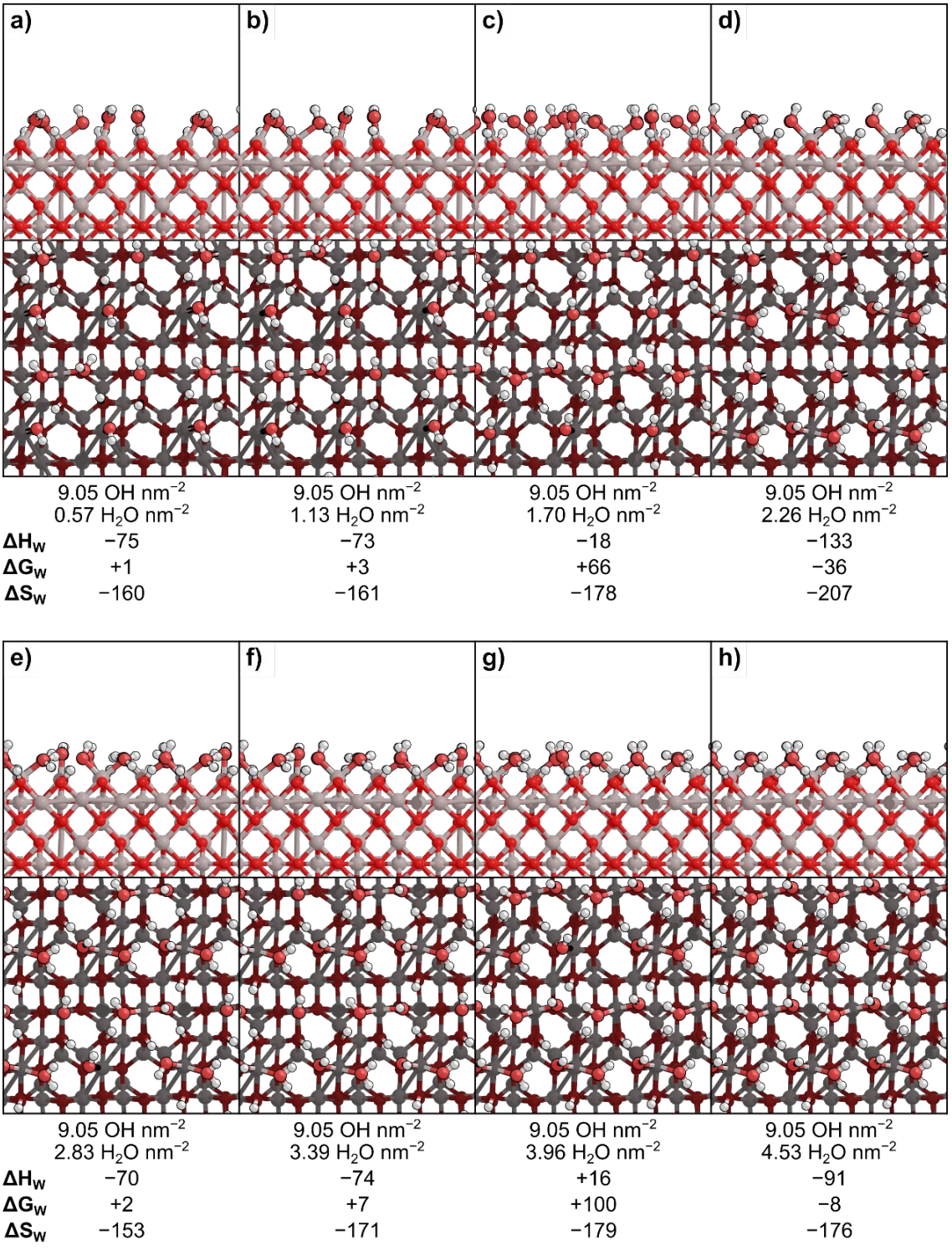

Figure S6. γ-Al_2O_3 with 9.05 OH nm^{-2} from dissociatively adsorbed H_2O and with (**a**) 0.56 H_2O nm^{-2}, (**b**) 1.13 H_2O nm^{-2}, (**c**) 1.70 H_2O nm^{-2}, (**d**) 2.26 H_2O nm^{-2}, (**e**) 2.83 H_2O nm^{-2}, (**f**) 3.39 H_2O nm^{-2}, (**g**) 3.96 H_2O nm^{-2}, and (**h**) 4.53 H_2O nm^{-2} (from 8 dissociatively and 1-8 more molecularly adsorbed H_2O molecules), shown parallel (top) and perpendicular (bottom) to the surface. Adsorption enthalpies (ΔH_W) and free energies (ΔG_W) in kJ mol^{-1} and entropies (ΔS_W) in J mol^{-1} K^{-1} are shown beneath each structure.

Calculations of H_2O adsorption near the HO–$Rh(CO)_2$ were completed with 0–7 dissociated H_2O (0–7.92 OH nm^{-2}) and, once H_2O begins to adsorb molecularly above this coverage, 0–20 molecularly adsorbed H_2O (0–11.31 H_2O nm^{-2}). The Rh, CO molecules, and all H*, OH*, and H_2O* on the γ-Al_2O_3 were permitted to vibrate in frequency calculations up to a total coverage of 7.92 OH nm^{-2} and 2.83 H_2O nm^{-2} (Fig. S7–S8). Above this coverage, only the $Rh(CO)_2$ was permitted to vibrate to test the effects of an H_2O overlayer on CO* frequencies (Fig. S9–S10). We exclude H_2O vibrational frequencies from these high coverages because the surface was predicted to saturate below this coverage under most conditions (absent the presence of liquid H_2O) and because such calculations are computationally expensive. Similarly, calculations for H_2O adsorption around HO–Rh(CO) (Fig. S11–S12) and HO–Rh were only performed up to a total coverage of 7.92 OH nm^{-2} and 2.83 H_2O nm^{-2} because H_2O is unlikely to exist above these coverages near these Rh structures.

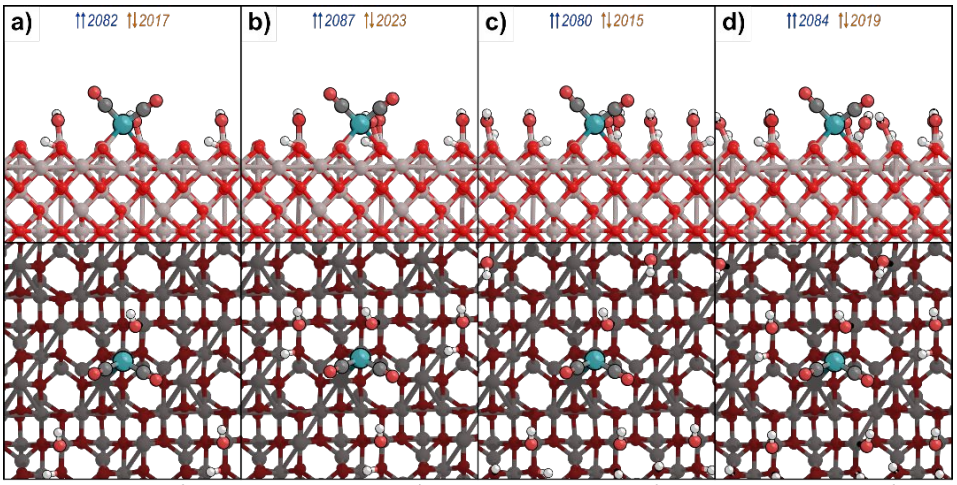

	1.13 OH nm^{-2} 0.00 H_2O nm^{-2}	2.26 OH nm^{-2} 0.00 H_2O nm^{-2}	3.39 OH nm^{-2} 0.00 H_2O nm^{-2}	4.53 OH nm^{-2} 0.00 H_2O nm^{-2}
ΔH_W	−143	−140	−127	−131
ΔG_W	−69	−66	−59	−57
ΔS_W	−157	−156	−143	−157
$\Delta H_{CO,2}$	−172	−138	−136	−125
$\Delta G_{CO,2}$	−105	−69	−71	−67
$\Delta S_{CO,2}$	−105	−107	−100	−86

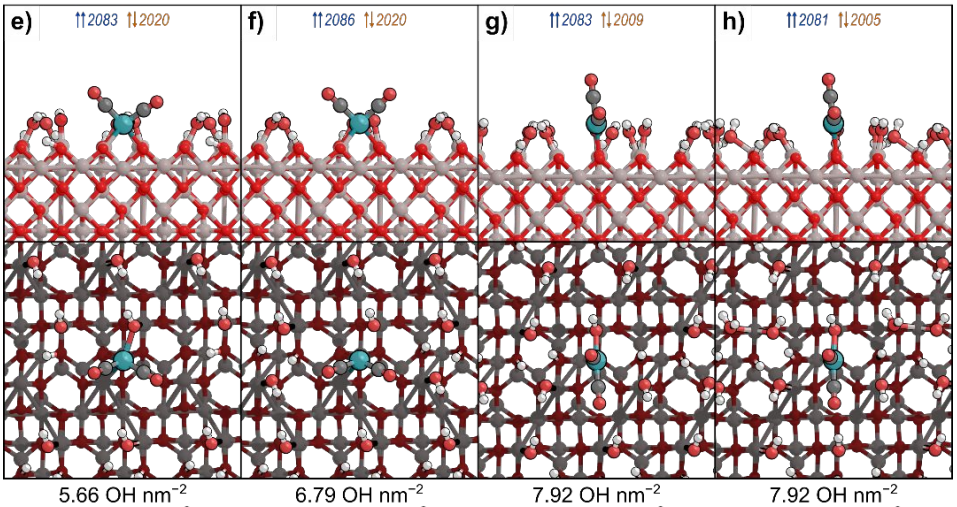

	5.66 OH nm^{-2} 0.00 H_2O nm^{-2}	6.79 OH nm^{-2} 0.00 H_2O nm^{-2}	7.92 OH nm^{-2} 0.00 H_2O nm^{-2}	7.92 OH nm^{-2} 0.57 H_2O nm^{-2}
ΔH_W	−128	−121	−97	−81
ΔG_W	−49	−51	−31	−4
ΔS_W	−168	−150	−140	−162
$\Delta H_{CO,2}$	−129	−128	−106	−107
$\Delta G_{CO,2}$	−61	−54	−36	−46
$\Delta S_{CO,2}$	−107	−121	−110	−92

Figure S7. γ-$Al_2O_3(010)_b$ with $Rh(CO)_2$ and with (**a**) 1.13 OH nm^{-2}, (**b**) 2.26 OH nm^{-2}, (**c**) 3.39 OH nm^{-2}, (**d**) 4.53 OH nm^{-2}, (**e**) 5.66 OH nm^{-2}, (**f**) 6.79 OH nm^{-2}, (**g**) 7.92 OH nm^{-2}, and (**h**) 7.92 OH nm^{-2} and 0.57 H_2O nm^{-2} from 1–7 dissociatively and 0–1 more molecularly adsorbed H_2O molecules, shown parallel (top) and perpendicular (bottom) to the surface. Adsorption enthalpies (ΔH) and free energies (ΔG) in kJ mol^{-1} and entropies (ΔS) in J mol^{-1} K^{-1} are shown beneath each structure for water (W subscript) and the second CO (CO,2 subscript). Calculated symmetric (blue) and asymmetric (orange) stretching frequencies are shown above each structure.

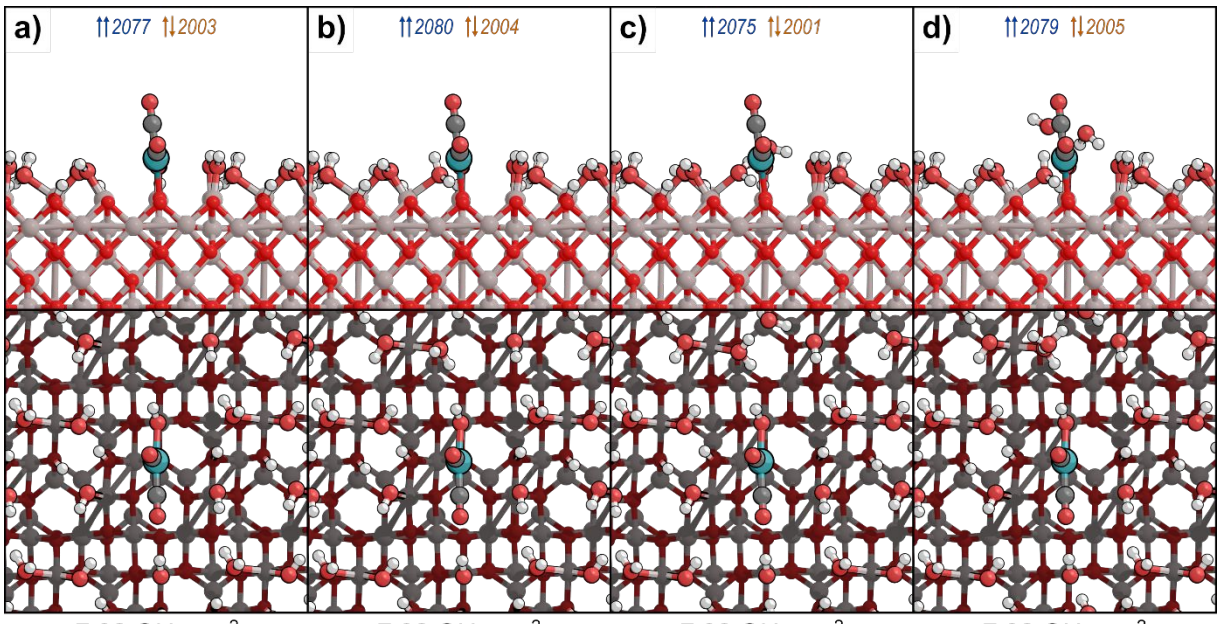

	7.92 OH nm^{-2} 1.13 H_2O nm^{-2}	7.92 OH nm^{-2} 1.70 H_2O nm^{-2}	7.92 OH nm^{-2} 2.26 H_2O nm^{-2}	7.92 OH nm^{-2} 2.83 H_2O nm^{-2}
ΔH_W	−81	−64	−67	−37
ΔG_W	−8	+9	+6	+36
ΔS_W	−154	−154	−154	−154
$\Delta H_{CO,2}$	−113	−116	−122	−122
$\Delta G_{CO,2}$	−54	−66	−78	−69
$\Delta S_{CO,2}$	−89	−69	−55	−76

Figure S8. γ-$Al_2O_3(010)_b$ with $Rh(CO)_2$ and with 7.92 OH nm^{-2} from 7 dissociatively adsorbed H_2O and (**a**) 1.13 H_2O nm^{-2}, (**b**) 1.70 H_2O nm^{-2}, (**c**) 2.26 H_2O nm^{-2}, (**d**) 2.83 H_2O nm^{-2} from 2–5 more molecularly adsorbed H_2O molecules, shown parallel (top) and perpendicular (bottom) to the surface. Adsorption enthalpies (ΔH) and free energies (ΔG) in kJ mol^{-1} and entropies (ΔS) in J mol^{-1} K^{-1} are shown beneath each structure for water (W subscript) and the second CO (CO,2 subscript). Calculated symmetric (blue) and asymmetric (orange) stretching frequencies are shown above each structure.

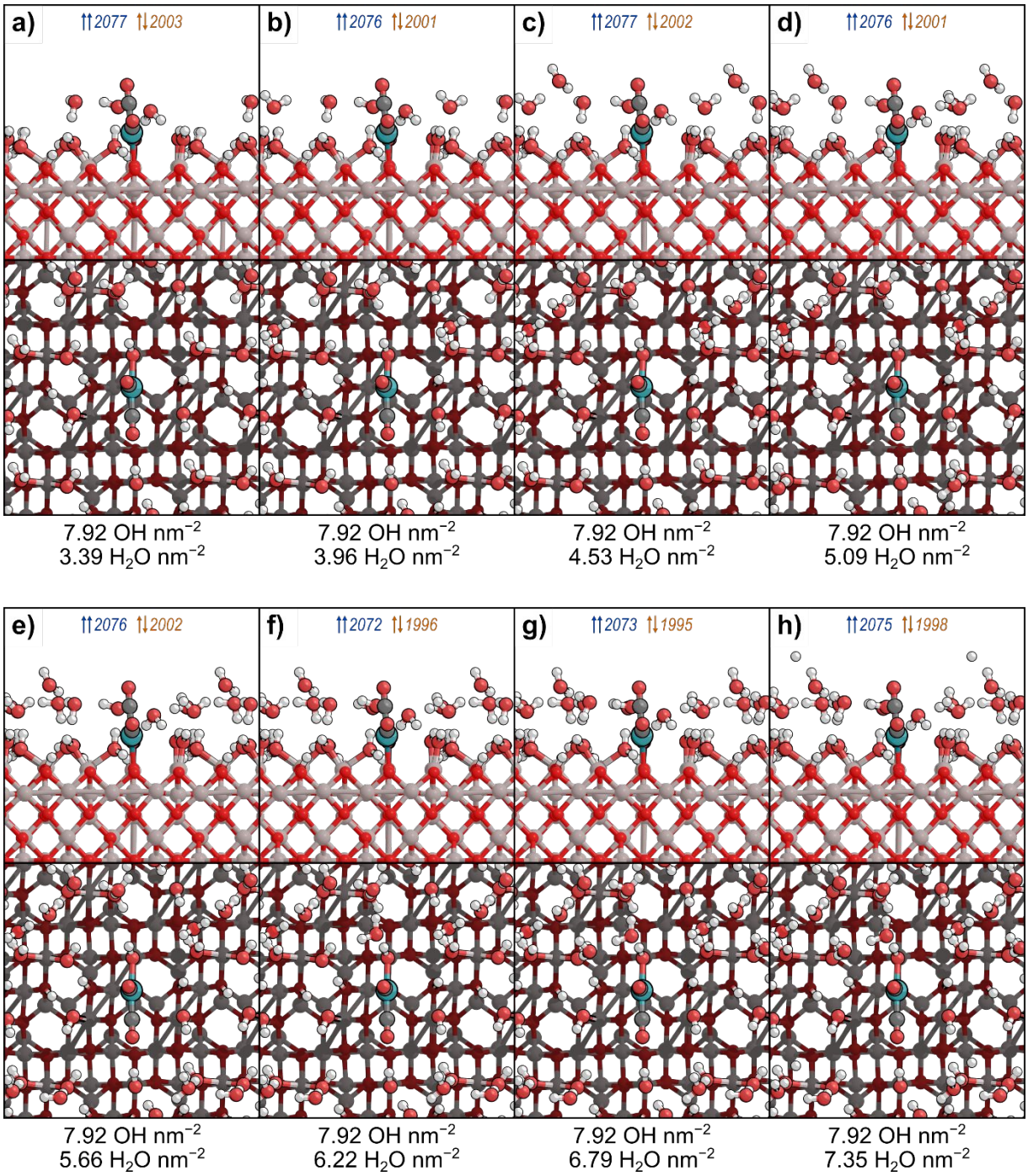

Figure S9. γ-$Al_2O_3(010)_b$ with $Rh(CO)_2$ and with 7.92 OH nm^{-2} from 7 dissociatively adsorbed H_2O and (**a**) 3.39 H_2O nm^{-2}, (**b**) 3.96 H_2O nm^{-2}, (**c**) 4.53 H_2O nm^{-2}, (**d**) 5.09 H_2O nm^{-2}, (**e**) 5.66 H_2O nm^{-2}, (**f**) 6.22 H_2O nm^{-2}, (**g**) 6.79 H_2O nm^{-2}, and (**h**) 7.35 H_2O nm^{-2} from 6–13 molecularly adsorbed H_2O molecules, shown parallel (top) and perpendicular (bottom) to the surface. Calculated symmetric (blue) and asymmetric (orange) stretching frequencies for the $Rh(CO)_2$ are shown above each structure.

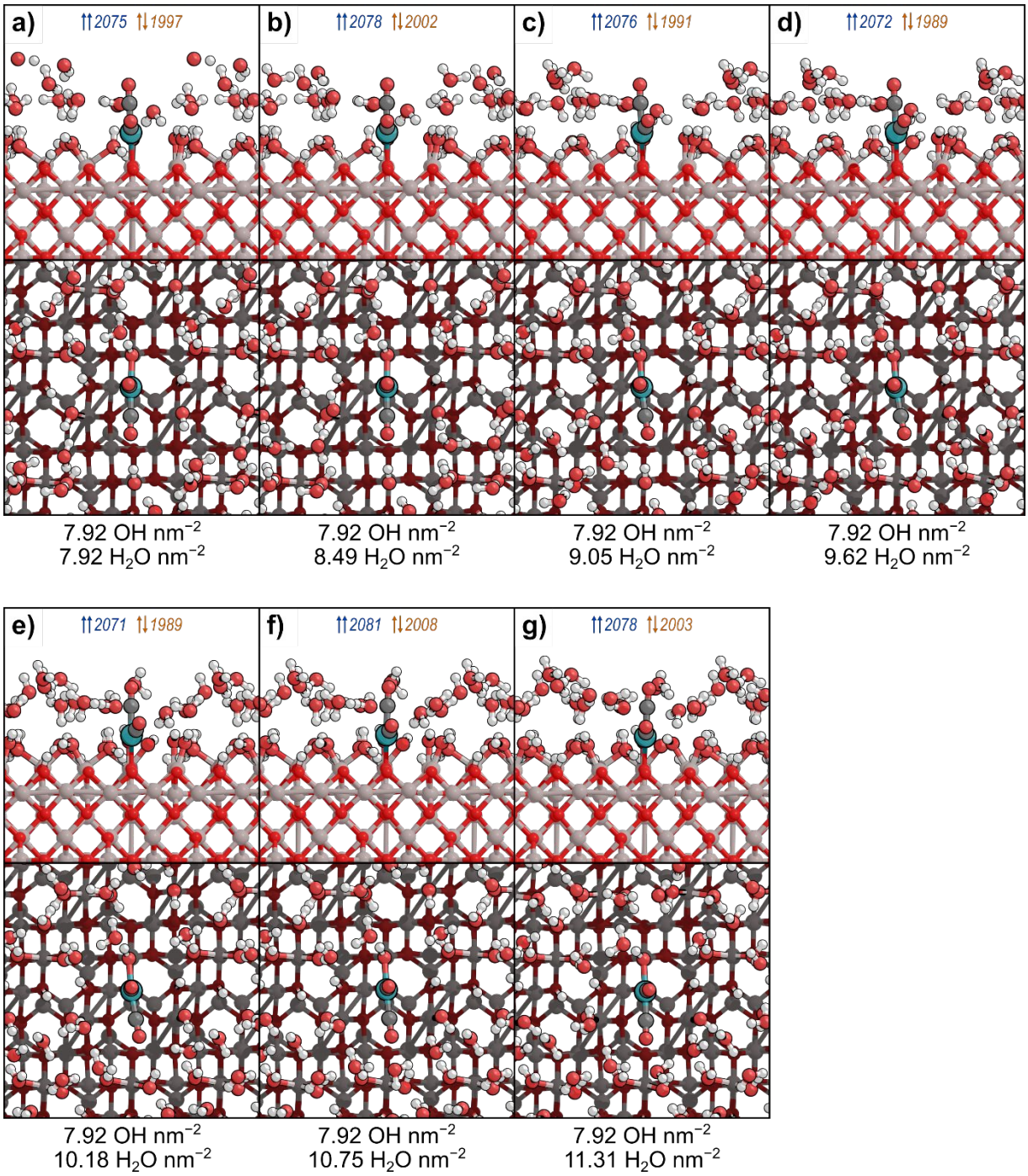

Figure S10. γ-$Al_2O_3(010)_b$ with $Rh(CO)_2$ and with 7.92 OH nm^{-2} from 7 dissociatively adsorbed H_2O and (**a**) 7.92 H_2O nm^{-2}, (**b**) 8.49 H_2O nm^{-2}, (**c**) 9.05 H_2O nm^{-2}, (**d**) 9.62 H_2O nm^{-2}, (**e**) 10.18 H_2O nm^{-2}, (**f**) 10.75 H_2O nm^{-2}, and (**g**) 11.31 H_2O nm^{-2} from 14–20 molecularly adsorbed H_2O molecules, shown parallel (top) and perpendicular (bottom) to the surface. Calculated symmetric (blue) and asymmetric (orange) stretching frequencies for the $Rh(CO)_2$ are shown above each structure.

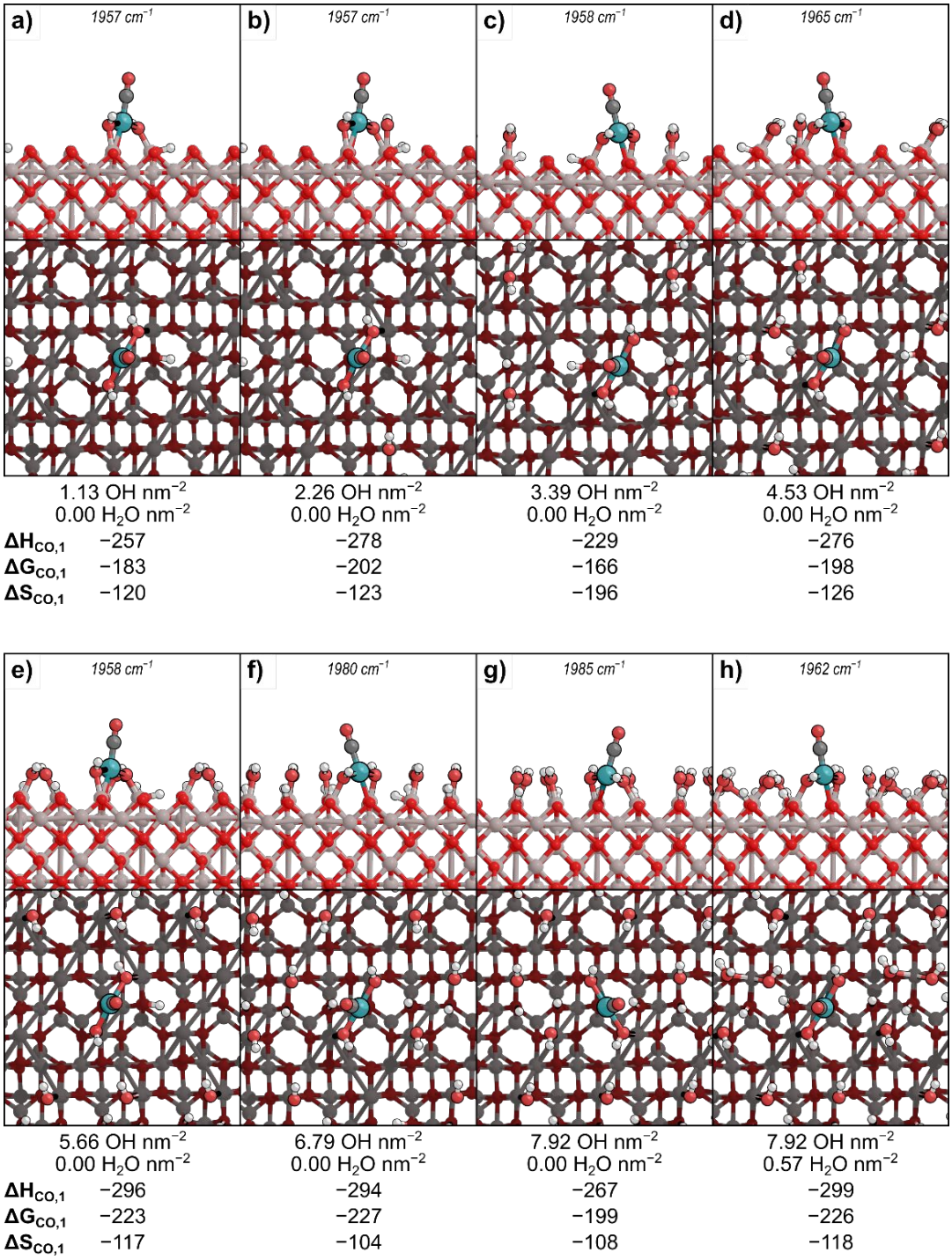

Figure S11. γ-$Al_2O_3(010)_b$ with Rh(CO) and with (**a**) 1.13 OH nm^{-2}, (**b**) 2.26 OH nm^{-2}, (**c**) 3.39 OH nm^{-2}, (**d**) 4.53 OH nm^{-2}, (**e**) 5.66 OH nm^{-2}, (**f**) 6.79 OH nm^{-2}, (**g**) 7.92 OH nm^{-2}, and (**h**) 7.92 OH nm^{-2} and 0.57 H_2O nm^{-2} from 1–7 dissociatively and 0–1 more molecularly adsorbed H_2O molecules, shown parallel (top) and perpendicular (bottom) to the surface. Adsorption enthalpies ($\Delta H_{CO,1}$) and free energies ($\Delta G_{CO,1}$) in kJ mol^{-1} and entropies ($\Delta S_{CO,1}$) in J mol^{-1} K^{-1} are shown beneath each structure for the first CO. Calculated CO stretching frequencies are shown above each structure.

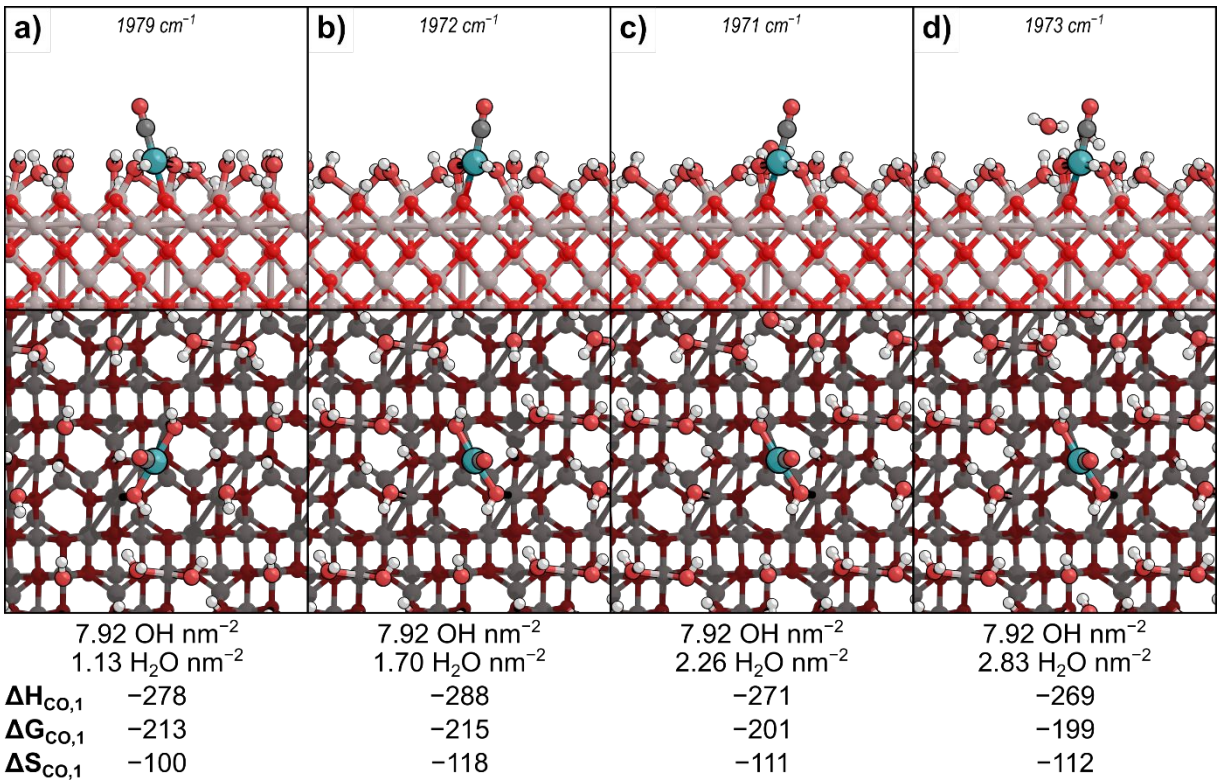

Figure S12. γ-$Al_2O_3(010)_b$ with Rh(CO) and with 7.92 OH nm^{-2} from 7 dissociatively adsorbed H_2O and (**a**) 1.13 H_2O nm^{-2}, (**b**) 1.70 H_2O nm^{-2}, (**c**) 2.26 H_2O nm^{-2}, (**d**) 2.83 H_2O nm^{-2} from 2–5 more molecularly adsorbed H_2O molecules, shown parallel (top) and perpendicular (bottom) to the surface. Adsorption enthalpies ($\Delta H_{CO,1}$) and free energies ($\Delta G_{CO,1}$) in kJ mol^{-1} and entropies ($\Delta S_{CO,1}$) in J mol^{-1} K^{-1} are shown beneath each structure for the first CO. Calculated CO stretching frequencies are shown above each structure.

S6. DFT structures of Rh(CO) and $Rh(CO)_2$ with different ligands and γ-Al_2O_3 surfaces

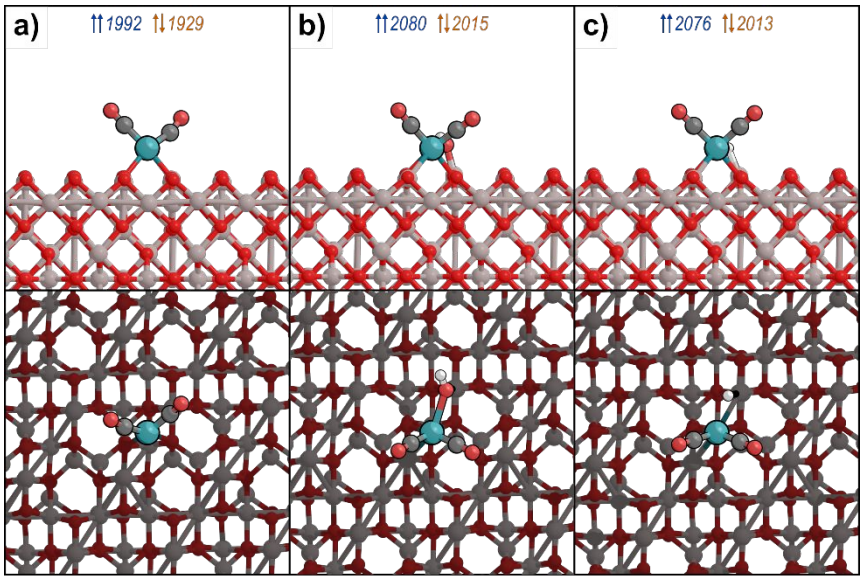

	No ligand	OH	H
$\Delta H_{CO,2}$	−105	−167	−74
$\Delta G_{CO,2}$	−37	−100	−2
$\Delta S_{CO,2}$	−143	−141	−153

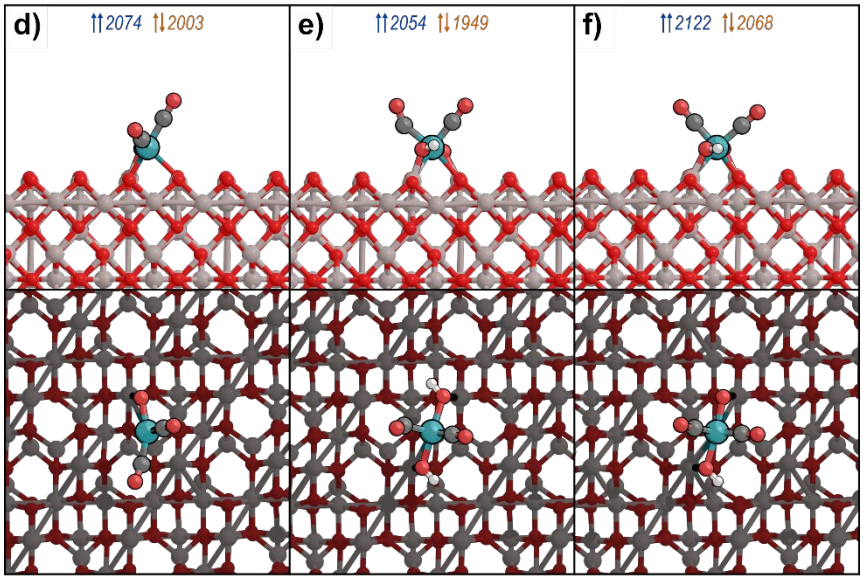

	O	2OH	O+OH
$\Delta H_{CO,2}$	−114	−27	−96
$\Delta G_{CO,2}$	−45	+37	−25
$\Delta S_{CO,2}$	−146	−136	−151

Figure S13. γ-$Al_2O_3(010)_b$ with $Rh(CO)_2$ and with (**a**) no ligand, (**b**) an OH^-, (**c**) an H^-, (**d**) an O^{2-}, (**e**) two OH^-, and (**f**) an O^{2-} and OH^-, shown parallel (top) and perpendicular (bottom) to the surface. Calculated symmetric (blue) and asymmetric (orange) stretching frequencies for the $Rh(CO)_2$ are shown above each structure.

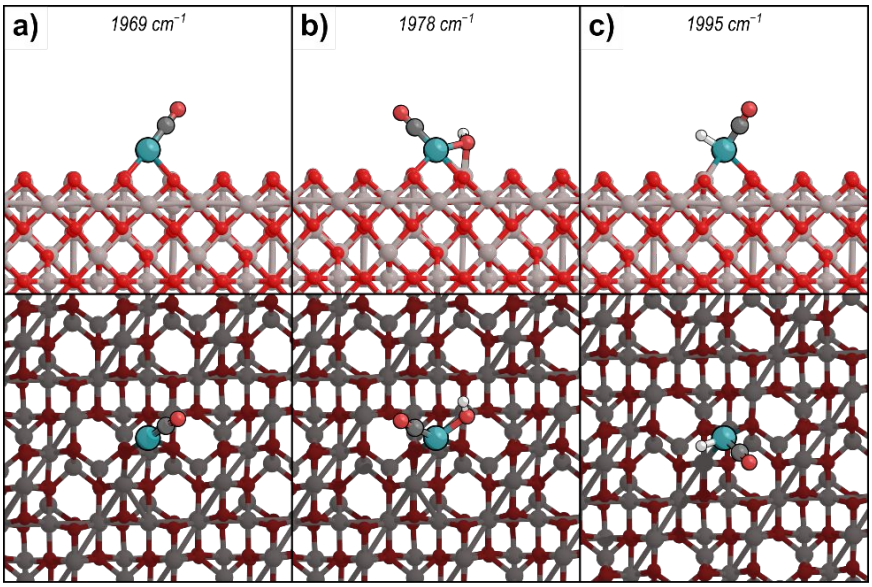

	No ligand	OH	H
$\Delta H_{CO,1}$	−275	−260	−278
$\Delta G_{CO,1}$	−202	−185	−206
$\Delta S_{CO,1}$	−153	−158	−151

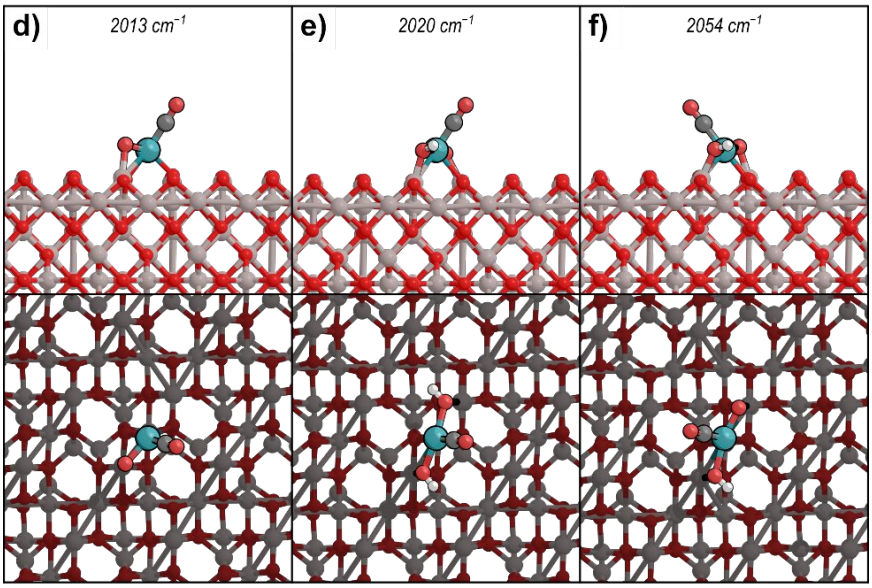

	O	2OH	O+OH
$\Delta H_{CO,1}$	−218	−210	−158
$\Delta G_{CO,1}$	−147	−137	−88
$\Delta S_{CO,1}$	−151	−153	−148

Figure S14. γ-$Al_2O_3(010)_b$ with Rh(CO) and with (**a**) no ligand, (**b**) an OH^-, (**c**) an H^-, (**d**) an O^{2-}, (**e**) two OH^-, and (**f**) an O^{2-} and OH^-, shown parallel (top) and perpendicular (bottom) to the surface. Calculated stretching frequencies for the Rh(CO) are shown above each structure.

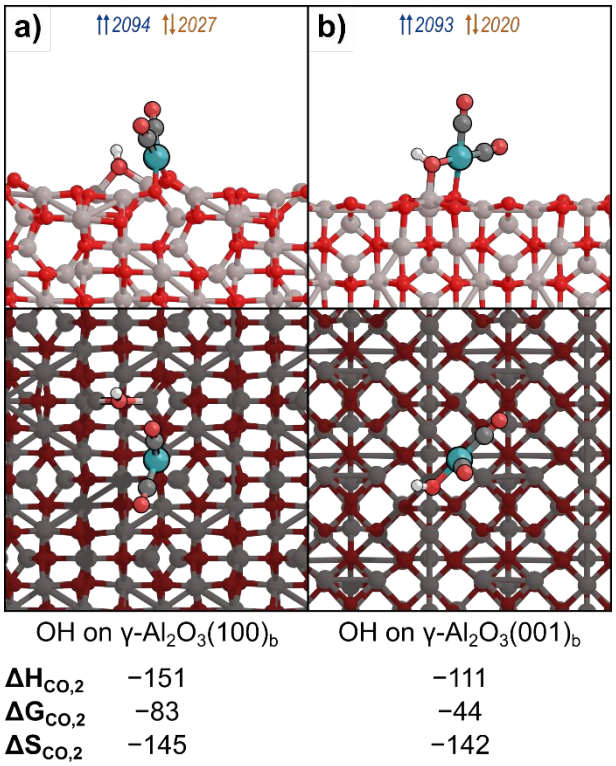

Figure S15. $Rh(CO)_2$ with an OH^- ligand on (**a**) γ-$Al_2O_3(100)_b$ and (**b**) γ-$Al_2O_3(001)_b$ shown parallel (top) and perpendicular (bottom) to the surface. Calculated symmetric (blue) and asymmetric (orange) stretching frequencies for the $Rh(CO)_2$ are shown above each structure.

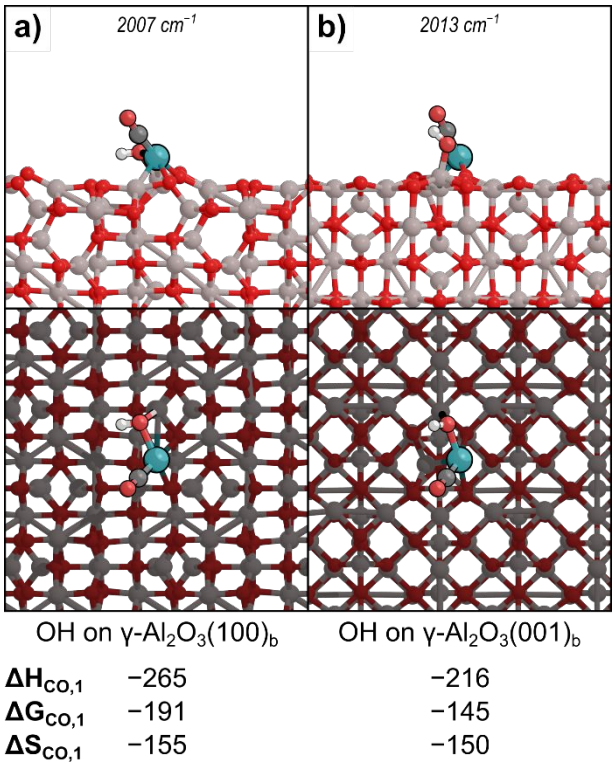

Figure S16. Rh(CO) with an OH^- ligand on (**a**) γ-$Al_2O_3(100)_b$ and (**b**) γ-$Al_2O_3(001)_b$ shown parallel (top) and perpendicular (bottom) to the surface. Calculated stretching frequencies for the Rh(CO) are shown above each structure.

References

(1) McQuarrie, D. A. *Statistical mechanics*; University Science Books: Sausalito, Calif, 2000.

(2) Digne, M.; Sautet, P.; Raybaud, P.; Euzen, P.; Toulhoat, H. *J. Catal.* **2002**, *211*, 1.

(3) Digne, M.; Sautet, P.; Raybaud, P.; Euzen, P.; Toulhoat, H. *J. Catal.* **2004**, *226*, 54.

(4) Raybaud, P.; Chizallet, C.; Mager-Maury, C.; Digne, M.; Toulhoat, H.; Sautet, P. *J. Catal.* **2013**, *308*, 328.

(5) Pigeon, T.; Chizallet, C.; Raybaud, P. *J. Catal.* **2021**.

(6) Gutiérrez, G.; Taga, A.; Johansson, B. *Phys. Rev. B* **2001**, *65*, 012101.

(7) Asokan, C.; Yang, Y.; Dang, A.; Getsoian, A. "Bean"; Christopher, P. *ACS Catal.* **2020**, *10*, 5217.

(8) Yoo, C.; Getsoian, A.; Bhan, A. *Appl. Catal. B* **2021**, 119893.